



Characterizations of calcium silicate hydrates derived from coal fly ash and their mechanisms for phosphate removal

Quanzhi Tian, Keiko Sasaki*

Department of Earth Resources Engineering, Faculty of Engineering, Kyushu University, 744 Motooka, Nishiku, Fukuoka 819-0395, Japan, email: tianqz0502@foxmail.com (Q. Tian), Tel. & Fax +81-92-802-3338, email: keikos@mine.kyushu-u.ac.jp (K. Sasaki)

Received 21 October 2018; Accepted 17 March 2019

ABSTRACT

Coal fly ash is an industrial waste generated from the thermal power plant and a large amount of it could be produced annually in the world, which can cause serious environmental problems. Reutilization of coal fly ash could be imperative to alleviate the environmental pressure. Thus, in the present study, coal fly ash was used as silicon source for the synthesis of calcium silicate hydrates (C-S-Hs) through the desilication process. Two kinds of C-S-Hs was synthesized at 100°C and room temperature respectively, with the fixed Ca/Si molar ratio of 1.2, and adopted as the adsorbents for phosphate. The properties of them were characterized using XRD, SEM, FTIR, TG-DTA as well as surface area and pore analysis. Compared to C-S-H synthesized from high temperature, the C-S-H obtained at room temperature possessed high purity and larger surface area. Therefore, synthesis by agitation at room temperature could be an alternative method to produce C-S-H materials from desilication liquid of coal fly ash, and this could save infrastructure cost and energy consumption. Both C-S-H materials have good ability to immobilize phosphate pollutant (higher than 100 mg·g⁻¹). The specific mechanisms of phosphate removal using C-S-H include several steps: firstly, phosphate ion was immobilized by binding with Ca²⁺ and forming aggregates, and the C-S-H structures were gradually corroded. Eventually, hydroxyapatite was formed after the C-S-H structure was totally destroyed.

Keywords: Coal fly ash; Calcium silicate hydrate; Phosphate removal

1. Introduction

Coal fly ash is a byproduct produced from thermal power plants, and every year a large amount of it is generated due to the world's reliance on coal-fired power generation [1]. Therefore, disposal of coal fly ash has been a serious problem all over the world. Reutilization of fly ash could be a good way to make a balance between economic and environmental benefits. It has been explored for various applications including cement additive, road base construction, soil amendment, zeolite and geopolymer synthesis [2]. However, there are still large amounts of coal fly ash disposed in landfill or ash pond. Thus, to develop new recycling methods for coal fly ash is becoming imperative. In recent decades, more efforts have been made to the exploration of extracting aluminum from coal fly ash which

contains a very high content of aluminum (usually 40–55%) [1,3]. For this purpose, the process of pre-desilication is normally designed in order to reduce the silica content and the consumption of sintering mediums [4]. Thus, a considerable amount of waste liquid is generated in this process and still not effectively handled. Currently, the disposal of silicon-rich desilication liquids occurs to be a critical problem. The high-valuable utilization of waste liquids could be of great economic benefit as well as environmental significance. Calcium silicate hydrate (C-S-H) is the main content of cement hydration products. Importantly, it has much potential for environmental applications [5–8]. Thus, the desilication liquid could be a good silicon source for C-S-H synthesis, and this is also quite possible way to the effective utilization of desilication liquid [9,10].

Phosphorus (P) is an essential element for cellular metabolism of all living organisms and also an on-renewable and irreplaceable resource [11]. However, eutrophication of

*Corresponding author.

surface waters has led to serious environmental problems, which is mainly caused by excessive inputs of P from industrial or urban sewages [12]. Hence, P removal from wastewater before discharge has to be considered to protect natural water from eutrophication. Currently, various technologies including biological, chemical, and physical treatments have been proposed to remove P from wastewater [13]. Among these technologies, struvite ($\text{MgNH}_4\text{PO}_4 \cdot 6\text{H}_2\text{O}$) and hydroxyapatite ($\text{Ca}_{10}(\text{PO}_4)_6(\text{OH})_2$) crystallization are the two feasible methods for P recovery from wastewater [14]. Generally, struvite crystallization requires high concentrations of ammonium and magnesium ions, and has been applied to P recovery from an aerobic sludge digestion liquor in full-scale wastewater [15]. However, the obtained struvite cannot be used for phosphate chemical industry. As for hydroxyapatite, it can be used as the source for fertilizer production and phosphorus chemical industry. Furthermore, Zhang et al. [16] recovered the phosphate from wastewater by C-S-H and then adopted the P-riched hydroxyapatite to remove lead from aqueous solution, showing good performance. Thus, hydroxyapatite has more versatile applications in the manufacturing industry. On the other hand, C-S-H has been considered to be the promising materials for P removal and recovery [17, 18]. Zhang et al. [19] showed a good performance of P removal (109 mg/g) using synthesized C-S-H at room temperature. Li et al. [20] studied C-S-H adopted for immobilization of P in lake sediment and concluded that C-S-H could largely reduce the potential risk of P release from sediment. There are also other reports indicating that C-S-H has good immobilization ability for phosphorus [17,21,22]. Many C-S-Hs are synthesized from the natural siliceous substances or solid wastes, such as natural shale [17], carbide residue [23], slag [24], biomass ash [25,26] etc., which could make full use of these natural minerals or wastes. However, there are few reports focusing on P removal and recovery using C-S-H synthesized from desilication liquid of coal fly ash. Therefore, in the present work, the desilication liquid was obtained from alkali dissolution of coal fly ash, and used as raw material to prepare C-S-Hs. Two kinds of C-S-Hs were respectively synthesized at high temperature and room temperature. The properties of them were compared using XRD, FTIR, TG-DTA as well as specific area and pore distribution. The P sorption performance of both C-S-Hs was also compared and evaluated. Furthermore, the mechanisms of the immobilization process of P were discussed and speculated.

2. Experimental

2.1. Materials

The coal fly ash used in this study was collected from a thermal power plant in China. Fig. 1 shows its XRD pattern collected on a Rigaku Ultima IV XRD (Akishima, Japan): Cu $K\alpha$ (40 kV, 40 mA) with a Ni filter at a scanning speed of 2°min^{-1} and scanning step of 0.02° . An indistinct swell peak appeared in the angle from 20° to 30° , which indicated the existence of the amorphous substance in fly ash. There were also crystal minerals including quartz, mullite and magnetite. The specific desilication process was as follows: 20 g coal fly ash was blended with 200 g 20% NaOH (solid to liquid mass ratio: 1:10) in a Teflon beaker. Then, the mixture was stirred and reacted for 2 h at 100°C . Thereafter,

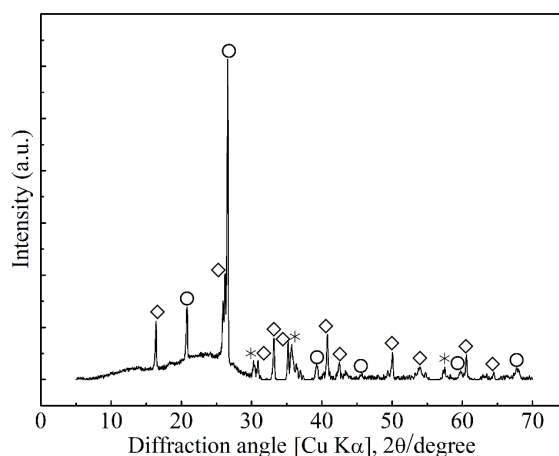


Fig. 1. XRD pattern of fly ash used in this study. Symbols: O, Quartz (SiO_2); \diamond , Mullite ($3\text{Al}_2\text{O}_3 \cdot 2\text{SiO}_2$); *, Magnetite (Fe_3O_4).

the mixture was cooled down to room temperature, and desilication liquid was obtained through a filtering process. The concentration of Si in this liquid was 9.65 mg/mL with impurities including Al (0.39 mg/mL), Ca (0.14 mg/mL), Mg (0.02 mg/mL) and Fe (0.17 mg/mL).

2.2. Preparation of C-S-Hs

To prepare C-S-Hs, two groups of 80 mL desilication-liquid were taken and reacted with 7.8102 g $\text{Ca}(\text{NO}_3)_2 \cdot \text{H}_2\text{O}$ (98.6%, Wako) where the ratio of Ca/Si was 1.2. One group of experiments was reacted at 100°C with the stirring speed of 400 rpm for 2 h and aged for another 18 h at the same temperature. The other reaction was put at room temperature with the agitation of 400 rpm for 7 d and parafilm was used to seal the beaker in order to avoid the contamination of carbon dioxide. After finishing the reaction process, both of them were washed using pure water until pH was lower than 10. The drying process was conducted in a vacuum dryer for 24 h and then solid powders were stored in glass bottles.

2.3. Sorption test

Removal of phosphate in solution was conducted to evaluate the sorption performances of the synthesized materials. Disodium hydrogen phosphate (Na_2HPO_4 , 99%, Wako) was used to prepare simulated phosphate wastewater. The sorption performance of the sorbent was evaluated by mixing the solids (50 mg) with test solution (50 mL) with P concentration of 200 mg/L for upto 24 h at 400 rpm. The sorption tests were conventionally performed at 25°C and initial pH of 7.0. The solutions were collected at different intervals including 5, 10, 20, 30 min and 1, 2, 3, 4, 5, 12, 24 h with the help of $0.2 \mu\text{m}$ filter to remove fine particles. The sorption capacity q_e (mg/g) was calculated using the following equation:

$$q_e = (C_0 - C_e)V / M \quad (1)$$

where C_0 and C_e (mg/L) are the concentrations of the solution at the initial and equilibrium stages, respectively. V (L)

is the volume of the test solution and M (g) is the mass of the used sorbent. Accordingly, sorbents after sorption at different intervals were collected and dried under vacuum, then subjected to XRD and FTIR measurements to confirm structural changes upon sorption time.

2.4. Characterizations

The concentrations of the elements including P, Ca and Si were determined using an inductively coupled plasma optical emission spectrometry (ICP-OES, Perkin Elmer, Optima 8300, US). XRD patterns of C-S-Hs and solid residues after P sorption were collected on a Rigaku Ultima IV XRD equipment as described above. Morphologies of C-S-Hs were observed by a VE-9800 SEM (Keyence, Osaka, Japan) with 20 kV acceleration voltages. TG-DTA (2000 SA thermal balance, Bruker, Germany) was used to determine their thermal properties with the α -Al₂O₃ as the reference material. Heating rate and airflow were 10°C/min and 100 mL·min⁻¹, respectively. The specific surface areas and pore size distributions of C-S-Hs were calculated according to the Brunauer-Emmett-Teller (BET method) and Barrett-Joyner-Halenda equations (BJH method) respectively, based on the N₂ adsorption-desorption curves which were measured on a high-precision surface area and pore size distribution analyzer (BEL-Max, BEL, Japan) at -196°C. Pre-treatment under vacuum at 100°C for 15 h was conducted in order to remove adsorbed gas and water. The FTIR spectra (400–4000 cm⁻¹) were recorded by an FTIR-spectrometer (JASCO 670 Plus, Japan) with a resolution of 4 cm⁻¹ using samples diluted by KBr.

3. Results and discussion

3.1. Characterizations of synthesized materials

Fig. 2 presents XRD patterns of C-S-Hs synthesized at different temperatures. Both of samples exhibited clear diffraction peaks at 29.3°, 32°, 49.8° and 55.1° which were well consistent with standard peaks of C-S-H [27], suggesting successful formations of C-S-H. For C-S-H obtained at a high temperature (HTC-S-H), hydroxycancrinite was also formed. Differently, the C-S-H synthesized at room temperature (RTC-S-H) presented almost pure phase. It can be known that the crystallinity of HTC-S-H was higher than that of RTC-S-H judged from the intensities and width of diffraction peaks. Therefore, high temperature could promote the reaction speed of C-S-H formation, but meanwhile, impurities would be generated. Generally, heating at high temperature is a common method to produce C-S-H [28,29]. However, from the view of engineering application, RTC-S-H is a more promising material for environmental applications because much more energy could be saved when synthesized at room temperature than that of heating at high temperature. In addition, SEM images of them are shown in Fig. 3. More folds exhibited on the surface of HTC-S-H, and the open framework structure could contribute to a large surface area and pore volume to which adsorbents were readily accessible. However, RTC-S-H seemed to be more solid, and the particle size was smaller than HTC-S-H. This could be due to the fact that C-S-H is the main content of cement hydration product and the degree of polymer-

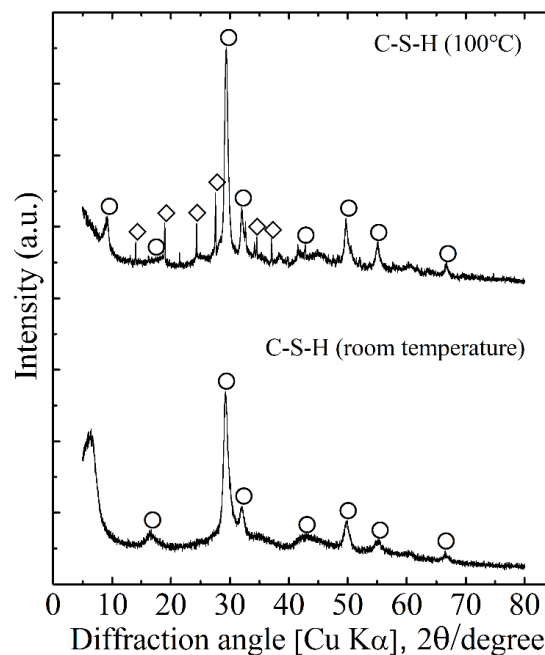


Fig. 2. XRD patterns of C-S-H derived from fly ash at 100°C and room temperature. Symbols: O, Calcium silicate hydrate (Ca/Si = 1.2–1.3); ◇, Hydroxycancrinite (Na₄(AlSiO₄)₃(OH)·(H₂O)).

ization of RTC-S-H might be higher than HTC-S-H [30,31].

N₂ adsorption-desorption isotherms of C-S-Hs were conducted and presented in Fig. 4. The two materials exhibited the typical nitrogen adsorption-desorption isotherms of calcium silicate hydrate. The steep rise at low relative pressure ($P/P_0 < 0.01$) corresponded to the filling of microstructure, while the hysteresis loop at relative pressures of $P/P_0 = 0.4–1$ reflected the existence of mesopores. The BET specific surface areas and average pore sizes of HTC-S-H and RTC-S-H were 56 m²/g; 33 nm, 64 m²/g; 29 nm, respectively. RTC-S-H had larger surface area than HTC-S-H, which could be attributed to the presence of more micropores.

TG-DTA curves for the materials are given in Fig. 5. It can be seen that each curve consisted of two zones. Generally, the dehydration of C-S-H happens between 100 and 300°C, and the surface adsorbed water is mainly removed below 100°C [32]. Thus, the exothermic peak appeared between 50 and 200°C. Compared to HTC-S-H, the weight loss of RTC-S-H below 100°C was higher, which was mainly because RTC-S-H contained a larger amount of free water than HTC-S-H. On the other hand, HTC-S-H contained impurities and this could also be a possible reason for its less weight loss. Another zone between 800 and 850°C was attributed to the formation of β -wollastonite (Ca₃(Si₃O₉)), which was an endothermic reaction [32].

FTIR spectra of synthesized materials are shown in Fig. 6. The peaks at 3468.17 cm⁻¹ and 3452.13 cm⁻¹ could be attributed to the stretching and bending vibrations of OH group [33]. The peaks at 1654.14 cm⁻¹ and 1657.72 cm⁻¹ were assigned to the OH bending vibration of hydroxyls or molecular H₂O. The strong bands at around 984 cm⁻¹ were asymmetrical stretching vibrations of O-Si-O. The deformation of Si-O-Si structure was represented at around 470 cm⁻¹ and symmet-

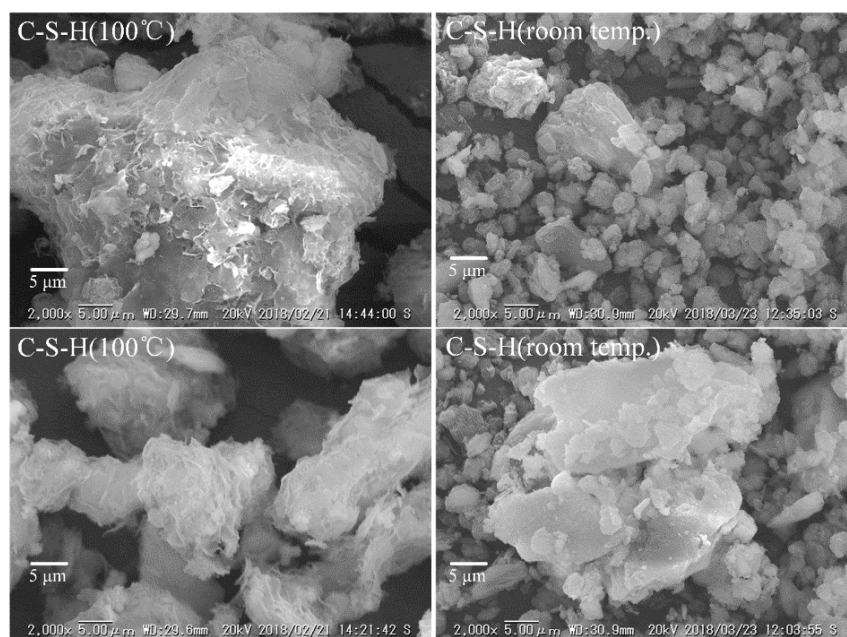


Fig. 3. SEM images of C-S-Hs derived from fly ash at 100°C and room temperature.

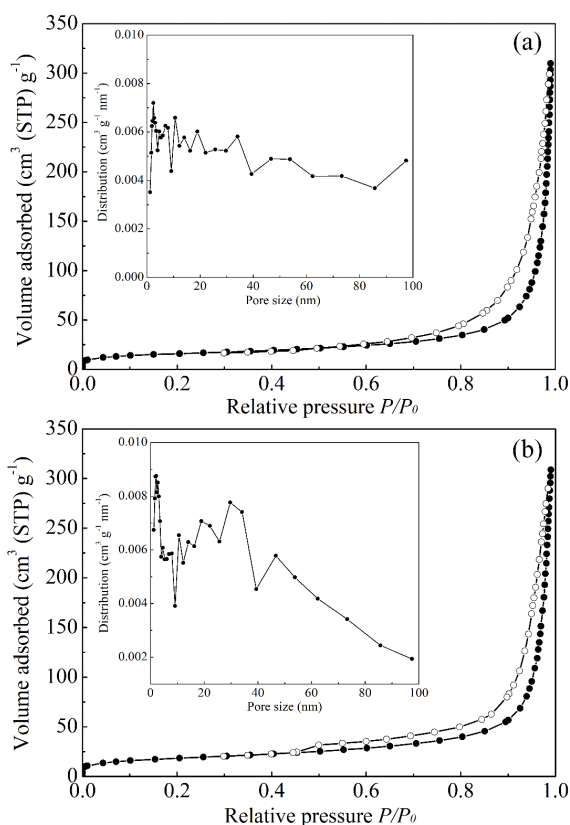


Fig. 4. Nitrogen adsorption–desorption isotherms of (a) C-S-H-100°C and (b) C-S-H-room temperature. Filled and empty symbols represent adsorption and desorption branches, respectively. The inset shows the corresponding pore size distribution curves determined by the BJH method using adsorption isotherms.

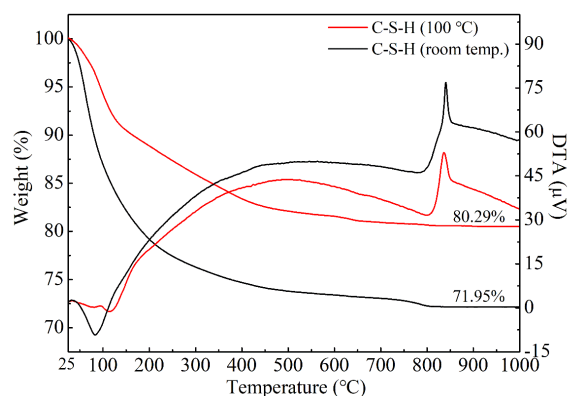


Fig. 5. TG-DTA curves of C-S-Hs derived from fly ash at 100°C and room temperature.

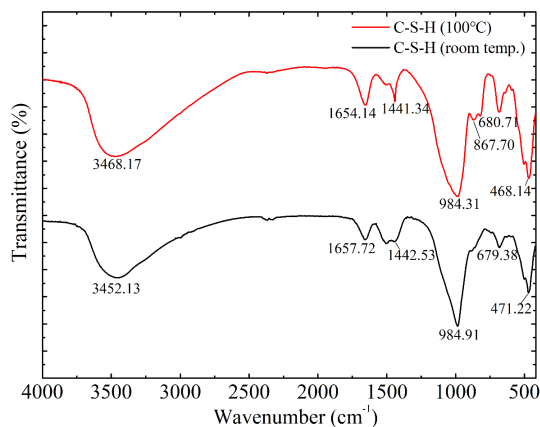


Fig. 6. FTIR spectra for C-S-Hs derived from fly ash at 100°C and room temperature.

rical vibration of Si-O-Si located at around 680 cm^{-1} [34]. The spectra of the two C-S-Hs presented almost the same positions in the peaks discussed above [35,36]. Therefore, it can be deduced that the basic frameworks of HTC-S-H and RTC-S-H were similar. On the other hand, the bands at 1441.34 cm^{-1} and 1442.53 cm^{-1} are characteristic bands assignable to antisymmetric stretching vibrations of CO_3 and the peak at 867.70 cm^{-1} belongs to its out-of-plane deformation vibration. These peaks can be obviously found in the spectra of HTC-S-H and RTC-S-H, which suggested that both C-S-Hs were easily contaminated by carbon dioxide.

3.2. Phosphate removal

The sorption of phosphate onto C-S-H vs. time is presented in Fig. 7. A sharp increase in sorption capacity (q_e) was observed during the first 30 min for both C-S-H compounds, and then the P sorption amounts lowly increased even after 6 h. The maximum sorption uptake of HTC-S-H in 24 h was determined to be $108\text{ mg}\cdot\text{g}^{-1}$, which was a little bit larger than that of RTC-S-H ($102\text{ mg}\cdot\text{g}^{-1}$). Generally, Ca^{2+} sites

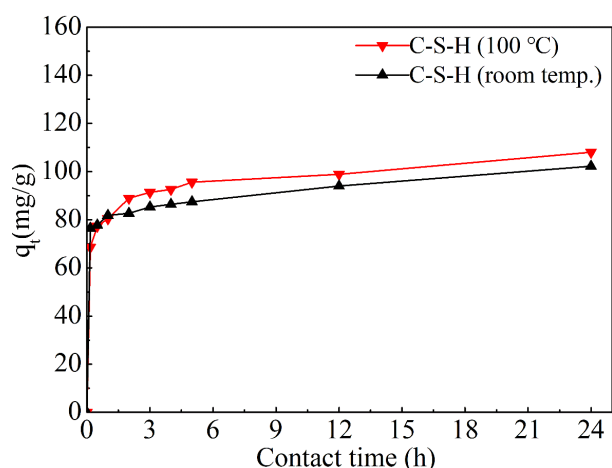


Fig. 7. Phosphate sorption capacity of C-S-Hs versus time.

embedded in the C-S-H network served as active sites for binding phosphate ions [22]. In the current study, RTC-S-H possessed larger surface area than HTC-S-H, which implied that more Ca^{2+} sites should exist on the surface of RTC-S-H. However, high phosphate sorption capacity occurred in the case of HTC-S-H. Thus, the mechanisms of phosphate removal process using C-S-H materials might be not only Ca^{2+} sorption. Even though it played an important role in the immobilization of P. The amounts of released Ca^{2+} and Si^{4+} from both C-S-Hs in the absence and presence of phosphate were compared (Fig. 8). In the absence of P (Fig. 8a), both C-S-Hs released a certain amount of Ca^{2+} and Si^{4+} . Under the same condition, more Ca^{2+} and Si^{4+} were released from RTC-S-H. When in the presence of P (Fig. 8b), all of Ca^{2+} participated in the phosphate immobilization process because there was almost no Ca^{2+} in the solution. At the same time, more Si^{4+} was released from HTC-S-H. It seemed that more phosphate was sorbed onto HTC-S-H, which showed positive correlation with the released Si^{4+} . Thus, the relationship between released Si^{4+} and removed P was studied, shown in Fig. 9. For both C-S-H materials, approximately linear relationships were shown in the amounts of released Si^{4+} and removed P, which suggested that phosphate anion may replace silica tetrahedron in the structure of C-S-H, as literature [37] proposed. Therefore, phosphate removal process using C-S-H materials should include the process of calcium precipitation and silica tetrahedron replacement.

XRD patterns of solid residues of both C-S-H materials collected at different reaction times were examined (Fig. 10). The intensities of C-S-H peaks for both C-S-H adsorbents became lower with the increase of reaction time. Meanwhile, the formation of hydroxyapatite could be obviously observed in XRD pattern of solid residue collected after 24 h reaction. In the case of HTC-S-H (Fig. 10a), there was still hydroxycancrinite existed in the solid residue after 24 h reaction, which implied that it did not take part in the phosphate removal reaction. A new phase belonged to jaffeite ($\text{Ca}_4(\text{Si}_3\text{O}_7)(\text{OH})_6$) which was a kind of hydrated calcium silicate appeared after 0.5 h reaction, then the peak gradually disappeared with the increase of sorption time. This might be because the new phase was

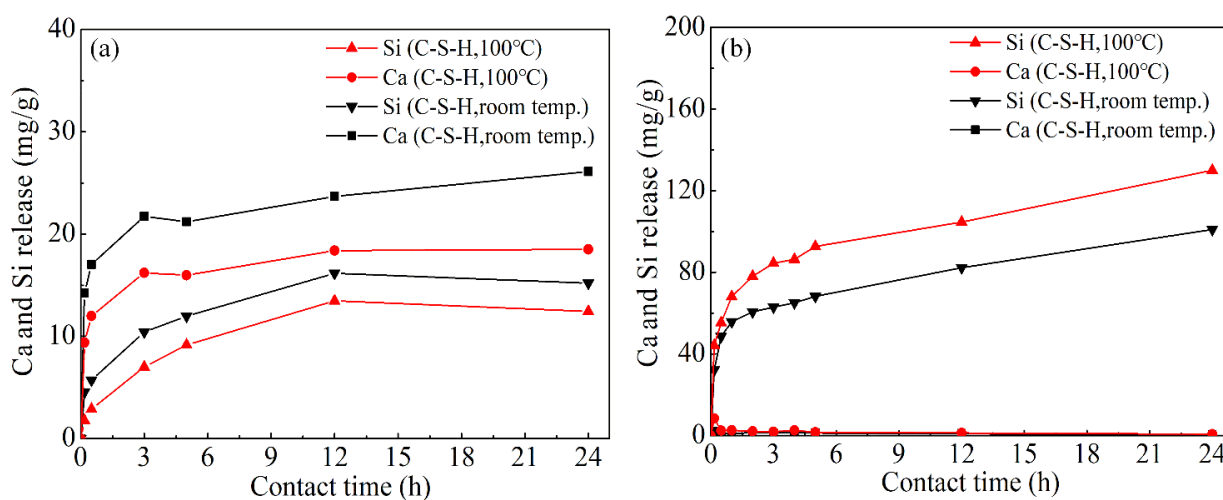


Fig. 8. Amounts of Ca and Si released from C-S-Hs in the absence (a) and presence (b) of P.

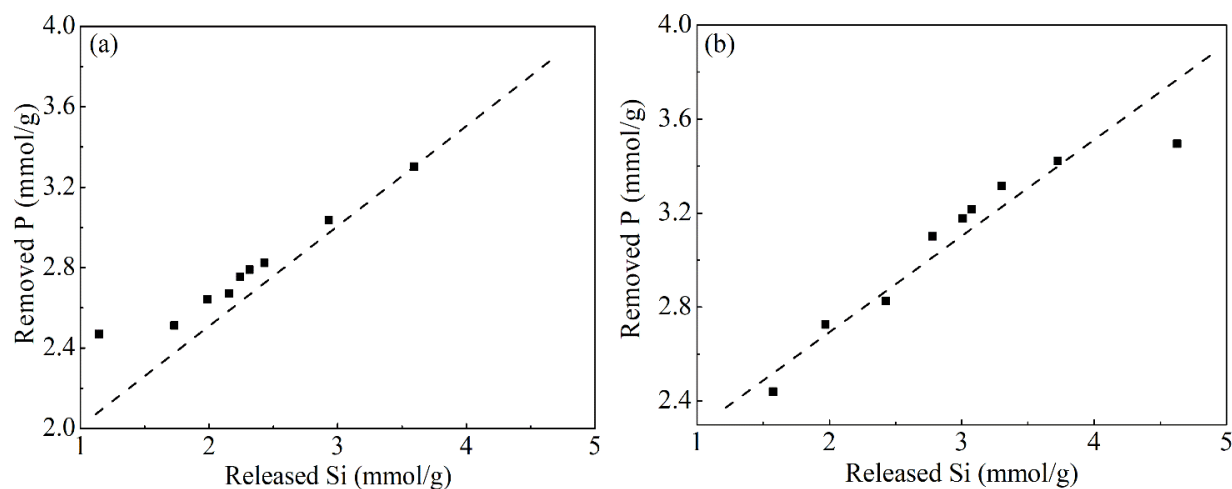


Fig. 9. Relationships between released Si and removed P. (a) C-S-H-100°C, (b) C-S-H-room temperature.

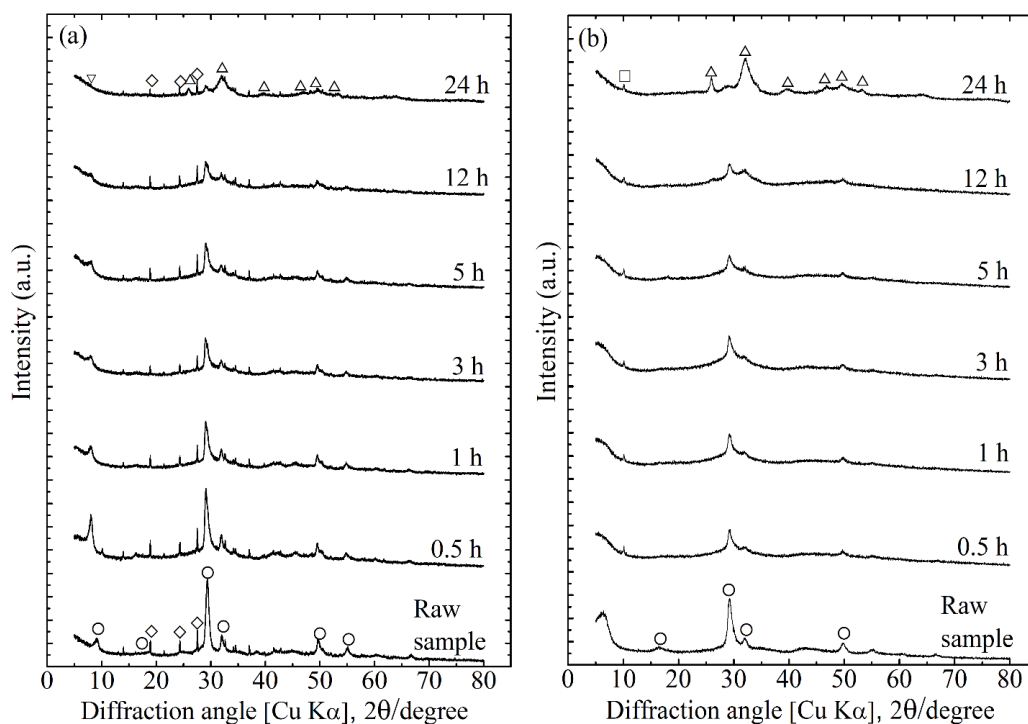


Fig. 10. Changes in XRD patterns of solid residues collected at different intervals in the presence of P. (a) C-S-H-100°C, (b) C-S-H-room temperature. Symbols: O, Calcium silicate hydrate ($\text{Ca}/\text{Si} \approx 1.2$); ◇, Hydroxycancrinite ($\text{Na}_4(\text{AlSiO}_4)_3(\text{OH}) \cdot (\text{H}_2\text{O})$); △, hydroxyapatite ($\text{Ca}_{10}(\text{PO}_4)_6(\text{OH})_2$); □, Jaffeite ($\text{Ca}_4(\text{Si}_3\text{O}_7)(\text{OH})_6$); ▽, Jennite ($\text{Ca}_9\text{Si}_6\text{O}_{18}(\text{OH})_6 \cdot 8\text{H}_2\text{O}$).

formed after HTC-S-H released excess Ca^{2+} and Si^{4+} and then destroyed by phosphate exchanging with silica tetrahedron. A similar situation occurred in the case of RTC-S-H (Fig. 10b). Another kind of hydrated calcium silicate (Jennite, $\text{Ca}_9\text{Si}_6\text{O}_{18}(\text{OH})_6 \cdot 8\text{H}_2\text{O}$) was formed and it existed during the whole reaction in a small amount. From the XRD analysis, the peak of hydroxyapatite did not appear until the sorption time reached up to 24 h. Thus, adsorption, precipitation and phase transformation should be included in the phosphate removal process by C-S-Hs. In addition to XRD

analysis, FTIR was used to characterize these solid residues, shown in Fig. 11. FTIR spectrum of the reference sample shows characteristic bands of phosphate occurring in ν_1 -963 cm^{-1} , ν_3 -1036 and 1095 cm^{-1} , ν_4 -568 and 600 cm^{-1} [38]. With the increase of sorption time, the peaks signified by dotted line changed gradually for both C-S-H adsorbents, which was in agreement with XRD analysis. Combined with the analysis of sorption results, phosphate could be sorbed on the C-S-H within a short time. The FTIR spectra showed a fuzzy peak at the position of the green dotted line in 0.5 h.

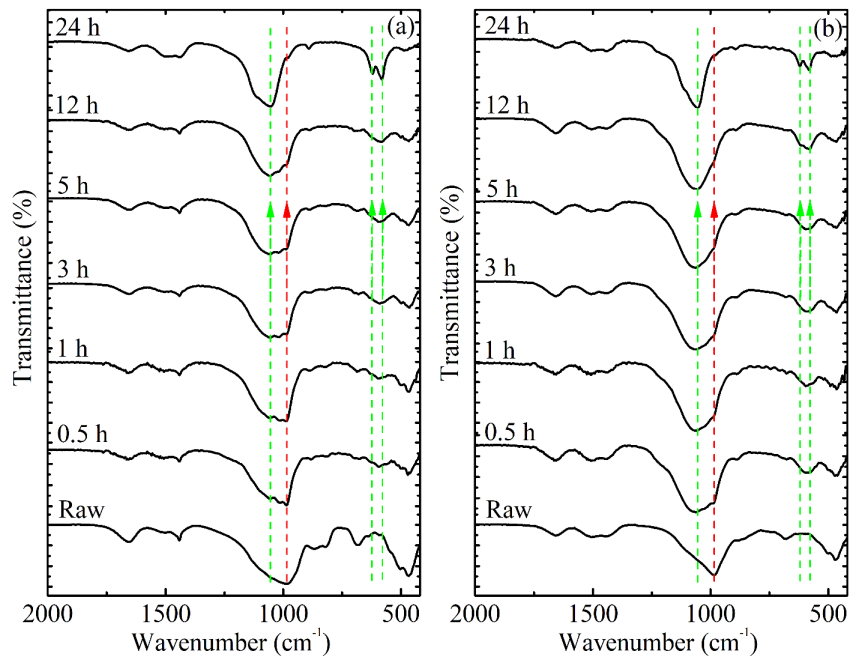


Fig. 11. Changes of FTIR spectra of solid residues collected at different reaction times. (a) C-S-H-100°C, (b) C-S-H-room temperature; The green dotted line represented the corresponding characteristic bands of P-O and red dotted line stood for stretching vibrations of Si-O.

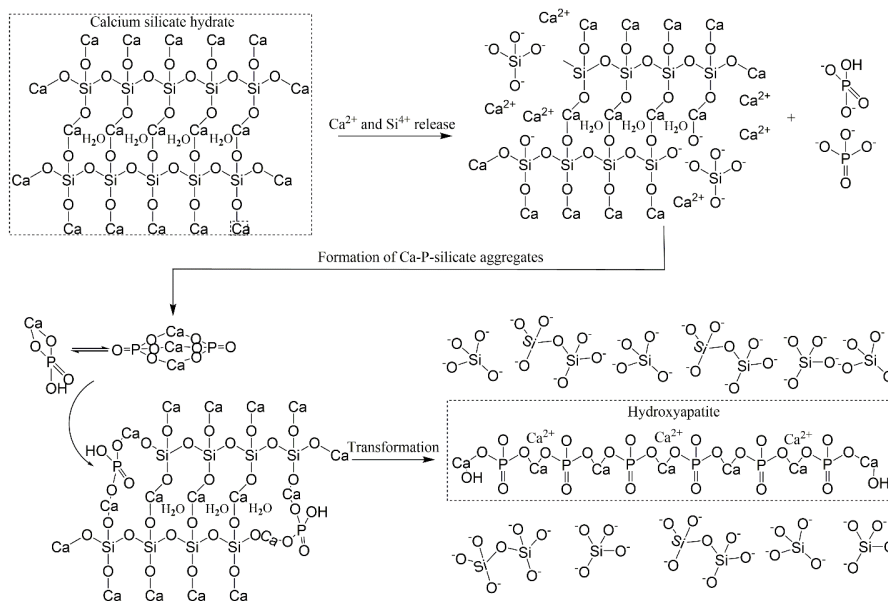


Fig. 12. The possible mechanisms of phosphate removal using calcium silicate hydrate.

However, there was no big difference between the XRD patterns of solid residue collected at 0.5 h and original material. This situation was maintained until the sorption time of 12 h for HTC-S-H and 5 h for RTC-S-H. There had been a broad peak corresponding to hydroxyapatite when the sorption time was 12 h in the case of RTC-S-H. The different changes in XRD could be due to the fact that the crystallinity of HTC-S-H was higher than RTC-S-H, which indicated that the structure of HTC-S-H was more stable than RTC-S-H. This led to the lower sorption amount of P using HTC-S-H

than RTC-S-H within the initial 1 h reaction. The removal of P using Ca-based materials has a close relationship with particle size, phase structure, etc. of used materials [39]. Small particle size can improve the speed of releasing Ca from solid, so the crystallization rate would be faster in the initial reaction stage. Referring to the large particle size, it can promote the crystallization rate in the later stage. This is consistent with the characterizations and sorption results.

In terms of phosphate immobilization mechanism, almost same transformation process happened as for both C-S-H

materials. Based on the analysis of XRD and FTIR results, and previous studies [12,18,24,37,40], the mechanisms of phosphate removal using C-S-H material are shown in Fig. 12. The acid dissociation constants indicate that the dominant phosphoric species are $[\text{HPO}_4]^{2-}$ in the pH range of 7–10 [41]. When C-S-H material was put into solution containing phosphate ions, the Ca^{2+} and Si^{4+} would be released and meanwhile $[\text{HPO}_4]^{2-}$ was quickly bound with Ca^{2+} into $\text{CaHPO}_4(\text{s})$ with $K_{\text{sp}} \approx 1.3 \cdot 10^{-7}$. This process would occur during the whole reaction process. Meanwhile, $\text{CaHPO}_4(\text{s})$ could be easily transformed into more stable compounds, such as $\text{Ca}_3(\text{PO}_4)_2$ ($K_{\text{sp}} = 1.2 \cdot 10^{-29}$), in the amorphous state under the pH of higher than 9. On the other hand, although hydroxyapatite (HAP) has a low solubility ($K_{\text{sp}} = 6.8 \cdot 10^{-37}$), these two compounds including CaHPO_4 and $\text{Ca}_3(\text{PO}_4)_2$ did not undergo transformation into more stable hydroxyapatite at the initial reaction. After sorption for 24 h, hydroxyapatite was obviously observed in XRD patterns. During this time, the sorption amount of P only increased a little. Previous studies [37] showed that $[\text{Ca}^{2+}-(\text{HPO}_4)^{2-}-\text{Ca}^{2+}]^{2+}$ aggregates could be formed at the initial stage of nucleation of Ca-P_i in aqueous solution. This aggregate was possible to bind to the negatively-charged C-S-H, forming Ca-P_i -silicate ion aggregate. From FTIR results, there was almost no stretching vibrations of Si-O appeared in the solid residue collected after sorption for 24 h. It could be known that almost all of the silicon had been released into solution. Thus, the removal mechanism should be as follow: phosphate ion was firstly immobilized by binding with Ca^{2+} and forming aggregates and it gradually corroded the structure of C-S-Hs. Eventually, hydroxyapatite was formed after the C-S-H structure was totally destroyed.

4. Conclusions

Two kinds of calcium silicate hydrates (C-S-Hs) were synthesized from the desilication liquid of coal fly ash with the fixed Ca/Si ratio of 1.2, and characterized by XRD, SEM, FTIR, TG-DTA as well as surface area and pore analysis. The results indicate that C-S-H synthesized at room temperature has a larger surface area and less impurities. Taking the infrastructure cost and energy consumption into consideration, C-S-H synthesis by agitation at room temperature should be a promising method to produce C-S-H materials from desilication liquid of coal fly ash. Both C-S-H materials have good ability to immobilize phosphorus in wastewater. Furthermore, the specific mechanisms of phosphate immobilization include several steps: phosphate ion was firstly immobilized by binding with Ca^{2+} and forming aggregates, and it gradually corroded the structure of C-S-Hs. Eventually, hydroxyapatite was formed after the C-S-H structure was totally destroyed. In the present study, we used the pure chemicals of P as the simulated pollutants to complete the sorption tests. However, real wastewater always contains many other anions or cations which definitely influence the P removal process using C-S-H. Next plan will be conducted to explore the effect of competitive ions on the P removal process by C-S-H materials.

Acknowledgments

This research was supported to KS by the JSPS (Japan Society for the Promotion of Science) Kaken Kiban A proj-

ect (No. JP16H02435) and to QT by the China Scholarship Council (No. 201706420068).

References

- [1] Z.T. Yao, M.S. Xia, P.K. Sarker, T. Chen, A review of the alumina recovery from coal fly ash, with a focus in China, *Fuel*, 120 (2014) 74–85.
- [2] Z.T. Yao, X.S. Ji, P.K. Sarker, J.H. Tang, L.Q. Ge, M.S. Xia, Y.Q. Xi, A comprehensive review on the applications of coal fly ash, *Earth-Sci. Rev.*, 141 (2015) 105–121.
- [3] A. Seidel, Y. Zimmels, Mechanism and kinetics of aluminum and iron leaching from coal fly ash by sulfuric acid, *Chem. Eng. Sci.*, 53 (1998) 3835–3852.
- [4] G.-h. Bai, T. Wei, X.-G. Wang, J.-G. Qin, X. Peng, P.-C. Li, Alkali desilicated coal fly ash as substitute of bauxite in lime-soda sintering process for aluminum production, *Trans. Nonfer. Metals Soc. China*, 20 (2010) s169–s175.
- [5] K. Barrera, A. Briso, V. Ide, L. Martorana, G. Montes, C. Basualto, T. Borrmann, F. Valenzuela, Treatment of acidic mine drainage in an adsorption process using calcium silicate modified with Fe (III), *Hydrometallurgy*, 172 (2017) 19–29.
- [6] H. Maeda, T. Abe, E.H. Ishida, T. Kasuga, Structure control of calcium silicate hydrate gels for dye removal applications, *J. Am. Ceram. Soc.*, 99 (2016) 2493–2496.
- [7] W. You, M. Hong, H. Zhang, Q. Wu, Z. Zhuang, Y. Yu, Functionalized calcium silicate nanofibers with hierarchical structure derived from oyster shells and their application in heavy metal ions removal, *PCCP*, 18 (2016) 15564–15573.
- [8] W. Guan, X. Zhao, Fluoride recovery using porous calcium silicate hydrates via spontaneous Ca^{2+} and OH^- release, *Sep. Purif. Technol.*, 165 (2016) 71–77.
- [9] J. Ma, G.T. Qin, Y.P. Zhang, J.M. Sun, S.L. Wang, L. Jiang, Heavy metal removal from aqueous solutions by calcium silicate powder from waste coal fly-ash, *J. Cleaner Prod.*, 182 (2018) 776–782.
- [10] G.X. Qi, X.F. Lei, L. Li, C. Yuan, Y.L. Sun, J.B. Chen, J. Chen, Y. Wang, J.M. Hao, Preparation and evaluation of a mesoporous calcium-silicate material (MCSM) from coal fly ash for removal of Co(II) from wastewater, *Chem. Eng. J.*, 279 (2015) 777–787.
- [11] E. Desmidt, K. Ghyselbrecht, Y. Zhang, L. Pinoy, B. Van der Bruggen, W. Verstraete, K. Rabaey, B. Meesschaert, Global phosphorus scarcity and full-scale P-recovery techniques: a review, *Crit. Rev. Environ. Sci. Technol.*, 45 (2015) 336–384.
- [12] U. Berg, D. Donnert, P. Weidler, E. Kaschka, G. Knoll, R. Nüesch, Phosphorus removal and recovery from wastewater by tobermorite-seeded crystallisation of calcium phosphate, *Water Sci. Technol.*, 53 (2006) 131–138.
- [13] W. Huang, Y. Zhang, D. Li, Adsorptive removal of phosphate from water using mesoporous materials: A review, *J. Environ. Manage.*, 193 (2017) 470–482.
- [14] M. Carballa, W. Moerman, W. De Windt, H. Grootaerd, W. Verstraete, Strategies to optimize phosphate removal from industrial anaerobic effluents by magnesium ammonium phosphate (MAP) production, *J. Chem. Technol. Biotechnol.*, 84 (2009) 63–68.
- [15] P. Cornel, C. Schaum, Phosphorus recovery from wastewater: needs, technologies and costs, *Water Sci. Technol.*, 59 (2009) 1069–1076.
- [16] Z. Zhang, X. Wang, H. Wang, J. Zhao, Removal of Pb(II) from aqueous solution using hydroxyapatite/calcium silicate hydrate (HAP/C-S-H) composite adsorbent prepared by a phosphate recovery process, *Chem. Eng. J.*, 344 (2018) 53–61.
- [17] K. Okano, M. Uemoto, J. Kagami, K. Miura, T. Aketo, M. Toda, K. Honda, H. Ohtake, Novel technique for phosphorus recovery from aqueous solutions using amorphous calcium silicate hydrates (A-CSHs), *Water Res.*, 47 (2013) 2251–2259.
- [18] Y. Kuwahara, S. Tamagawa, T. Fujitani, H. Yamashita, A novel conversion process for waste slag: synthesis of calcium silicate hydrate from blast furnace slag and its application as a versatile adsorbent for water purification, *J. Mater. Chem. A*, 1 (2013) 7199–7210.

- [19] Z. Zhang, X. Wang, J. Zhao, Phosphate recovery from wastewater using calcium silicate hydrate (CSH): sonochemical synthesis and properties, *Environ. Sci.: Water Res. Technol.*, 5 (2019) 131–139.
- [20] C. Li, H. Yu, S. Tabassum, L. Li, D. Wu, Z. Zhang, H. Kong, P. Xu, Effect of calcium silicate hydrates (CSH) on phosphorus immobilization and speciation in shallow lake sediment, *Chem. Eng. J.*, 317 (2017) 844–853.
- [21] Y. Zhao, H. Chen, Q. Yan, Enhanced phosphate removal during the simultaneous adsorption of phosphate and Ni^{2+} from electroless nickel wastewater by calcium silicate hydrate (CSH), *Environ. Technol. Innov.*, 8 (2017) 141–149.
- [22] H. Maeda, S. Yokota, T. Kasuga, Structural changes in calcium silicate hydrate gel and resulting improvement in phosphate species removal properties after mechanochemical treatment, *Royal Soc. Open Sci.*, 5 (2018) 181403.
- [23] W. Guan, F. Ji, Q. Chen, P. Yan, Q. Zhang, Preparation and phosphorus recovery performance of porous calcium-silicate-hydrate, *Ceram. Int.*, 39 (2013) 1385–1391.
- [24] Y. Kuwahara, H. Yamashita, Phosphate removal from aqueous solutions using calcium silicate hydrate prepared from blast furnace slag, *ISIJ Int.*, 57 (2017) 1657–1664.
- [25] X. Yao, K. Xu, Y. Liang, Comparing the thermo-physical properties of rice husk and rice straw as feedstock for thermochemical conversion and characterization of their waste ashes from combustion, *BioResources*, 11 (2016) 10549–10564.
- [26] X. Yao, K. Xu, Comparative study of characterization and utilization of corncob ashes from gasification process and combustion process, *Constr. Build. Mater.*, 119 (2016) 215–222.
- [27] M. Heikal, I. Helmy, H. El-Didamony, F.A. El-Raouf, Electrical properties, physico-chemical and mechanical characteristics of fly ash-limestone-filled pozzolanic cement, *Ceram. Silikaty*, 48 (2004) 49–58.
- [28] A. Hartmann, D. Schulenberg, J.-C. Buhl, Synthesis and structural characterization of CSH-phases in the range of $C/S = 0.41$ – 1.66 at temperatures of the tobermorite xonotlite crossover, *J. Mater. Sci. Chem. Eng.*, 3(11) (2015) 39–55.
- [29] G. Zhu, H. Li, X. Wang, S. Li, X. Hou, W. Wu, Q. Tang, Synthesis of calcium silicate hydrate in highly alkaline system, *J. Am. Ceram. Soc.*, 99 (2016) 2778–2785.
- [30] D. Macphee, E. Lachowski, F.P. Glasser, Polymerization effects in CSH: implications for Portland cement hydration, *Adv. Cement Res.*, 1 (1988) 131–137.
- [31] J.J. Thomas, H.M. Jennings, A colloidal interpretation of chemical aging of the CSH gel and its effects on the properties of cement paste, *Cem. Concr. Res.*, 36 (2006) 30–38.
- [32] R. Vedalakshmi, A.S. Raj, S. Srinivasan, K.G. Babu, Quantification of hydrated cement products of blended cements in low and medium strength concrete using TG and DTA technique, *Thermochim. Acta*, 407 (2003) 49–60.
- [33] P. Yu, R.J. Kirkpatrick, B. Poe, P.F. McMillan, X. Cong, Structure of calcium silicate hydrate (C-S-H): Near-, mid-, and far-infrared spectroscopy, *J. Am. Ceram. Soc.*, 82 (1999) 742–748.
- [34] R. Ylmén, U. Jäglid, B.-M. Steenari, I. Panas, Early hydration and setting of Portland cement monitored by IR, SEM and Vicat techniques, *Cem. Concr. Res.*, 39 (2009) 433–439.
- [35] I. Lognot, I. Klur, A. Nonat, NMR and infrared spectroscopies of CSH and Al-substituted CSH synthesised in alkaline solutions, *Nuclear Magnetic Resonance Spectroscopy of cement-based materials*, Springer, 1998, pp. 189–196.
- [36] M. Yousuf, A. Mollah, T.R. Hess, Y.-N. Tsai, D.L. Cocke, An FTIR and XPS investigations of the effects of carbonation on the solidification/stabilization of cement based systems-Portland type V with zinc, *Cem. Concr. Res.*, 23 (1993) 773–784.
- [37] K. Okano, S. Miyamaru, A. Kitao, H. Takano, T. Aketo, M. Toda, K. Honda, H. Ohtake, Amorphous calcium silicate hydrates and their possible mechanism for recovering phosphate from wastewater, *Sep. Purif. Technol.*, 144 (2015) 63–69.
- [38] A. Ślósarczyk, Z. Paszkiewicz, C. Paluszkiwicz, FTIR and XRD evaluation of carbonated hydroxyapatite powders synthesized by wet methods, *J. Mol. Struct.*, 744–747 (2005) 657–661.
- [39] W. Guan, F. Ji, D. Fang, Y. Cheng, Z. Fang, Q. Chen, P. Yan, Porosity formation and enhanced solubility of calcium silicate hydrate in hydrothermal synthesis, *Ceram. Int.*, 40 (2014) 1667–1674.
- [40] W. Guan, F. Ji, Q. Chen, P. Yan, W. Zhou, Phosphorus recovery using porous calcium silicate hydrate as seed crystal in form of hydroxyapatite, *Mater. Res. Innovations*, 18 (2014) 43–49.
- [41] M.A. Pasek, Rethinking early Earth phosphorus geochemistry, *Proceedings of the National Academy of Sciences*, 105 (2008) 853–858.